

# MICAL3 Flavoprotein Monooxygenase Forms a Complex with Centralspindlin and Regulates Cytokinesis<sup>\*[5]</sup>

Received for publication, July 13, 2016, and in revised form, August 12, 2016 Published, JBC Papers in Press, August 15, 2016, DOI 10.1074/jbc.M116.748186

Qingyang Liu<sup>†</sup>, Fan Liu<sup>§</sup>, Ka Lou Yu<sup>†1</sup>, Roderick Tas<sup>‡</sup>, Ilya Grigoriev<sup>‡</sup>, Sanne Remmelzwaal<sup>‡</sup>,  
 Andrea Serra-Marques<sup>‡2</sup>, Lukas C. Kapitein<sup>‡</sup>, Albert J. R. Heck<sup>§</sup>, and Anna Akhmanova<sup>‡3</sup>

From the <sup>†</sup>Cell Biology, Faculty of Science, Utrecht University, Padualaan 8, 3584 CH Utrecht and the <sup>§</sup>Biomolecular Mass Spectrometry and Proteomics, Bijvoet Center for Biomolecular Research and Utrecht Institute for Pharmaceutical Sciences, Utrecht University, 3584 CH Utrecht, The Netherlands

During cytokinesis, the antiparallel array of microtubules forming the central spindle organizes the midbody, a structure that anchors the ingressed cleavage furrow and guides the assembly of abscission machinery. Here, we identified a role for the flavoprotein monooxygenase MICAL3, an actin disassembly factor, in organizing midbody-associated protein complexes. By combining cell biological assays with cross-linking mass spectrometry, we show that MICAL3 is recruited to the central spindle and the midbody through a direct interaction with the centralspindlin component MKLP1. Knock-out of MICAL3 leads to an increased frequency of cytokinetic failure and a delayed abscission. In a mechanism independent of its enzymatic activity, MICAL3 targets the adaptor protein ELKS and Rab8A-positive vesicles to the midbody, and the depletion of ELKS and Rab8A also leads to cytokinesis defects. We propose that MICAL3 acts as a midbody-associated scaffold for vesicle targeting, which promotes maturation of the intercellular bridge and abscission.

Cytokinesis is the last step of cell division, during which the cytoplasm is partitioned between the two daughter cells. In animal cells, the major steps of cytokinesis are the formation of the actomyosin ring and its contraction, resulting in the ingression of the cleavage furrow, formation of an intercellular bridge, and its subsequent scission (1, 2). At the onset of cytokinesis, microtubules at the spindle midzone arrange into an overlapping antiparallel array, the central spindle, which first forms a signaling platform important for the positioning of the cleavage plane and later organizes the midbody, an electron-dense structure that anchors the ingressed furrow and guides the assembly of abscission machinery (1–3).

One of the major players in the assembly and function of the central spindle is the centralspindlin complex, composed of the kinesin-6 family protein mitotic kinesin-like protein 1 (MKLP1)<sup>4</sup> (also known as KIF23 in mammals) and the Rho GTPase activating protein CYK-4 (also known as or MgcRacGAP) (4). Centralspindlin participates in bundling antiparallel microtubules of the central spindle, activation of the Rho GTPase, which controls formation of the actomyosin ring, and the formation of the midbody (4).

Membrane trafficking, including both endosomes and secretory carriers, also plays an important role in cytokinesis (5–7). The small GTPase Rab8, known to label both endosomal and secretory vesicles (8–11), prominently accumulates at the midbody (12–14), and its transport to the intercellular bridge is directed by cytoplasmic dynein and the doublecortin domain-containing protein-5 (12). The docking and fusion of Rab8-positive secretory vesicles with the plasma membrane depends on the cortical complex, which contains a coiled-coil adaptor ELKS/ERC1 (15) and the flavoprotein monooxygenase enzyme MICAL3 (8). The members of the MICAL family, which in mammals includes MICAL1, MICAL2, and MICAL3, are best known for their ability to promote actin disassembly by oxidizing specific methionine residues (16–18). In addition, MICAL1 and MICAL3 can bind to multiple members of the Rab GTPase family, including Rab8 (8, 19), but the exact function of these interactions is poorly understood.

Here, we searched for new binding partners of MICAL3 and identified the two components of the centralspindlin complex among the highest hits. Because centralspindlin is a major player during cytokinesis, we hypothesized that MICAL3 also participates in this process. We tested this possibility using a combination of biochemical and cell biological experiments and found that MICAL3 is indeed required for cytokinesis. We showed that MKLP1 recruits MICAL3 to the central spindle, whereas MICAL3 participates in targeting to the midbody its binding partners ELKS and Rab8A, and the loss of both ELKS and Rab8A also caused cytokinesis defects. Interestingly, the cytokinetic function of MICAL3 appeared not to require its enzymatic activity. Our data suggest that MICAL3 plays a role in organizing membrane trafficking at the intercellular bridge

<sup>\*</sup> This work was supported by Netherlands Organization for Scientific Research Grant CW ECHO 711.011.005 (to A. A. and A. J. R. H.) and Proteins@Work, a program of the Netherlands Proteomics Centre financed by the Netherlands Organization for Scientific Research (NWO) as part of the National Roadmap Large-scale Research Facilities of the Netherlands Project Number 184.032.201. The authors declare that they have no conflicts of interest with the contents of this article.

[5] This article contains supplemental Movies S1–S3 and Table S1.

<sup>1</sup> Present address: Institute of Medical Biology, Agency for Science, Technology, and Research, Singapore, 8a Biomedical Grove, 06-06, Immunos, Singapore 138648.

<sup>2</sup> Present address: Dept. of Cell and Tissue Biology, University of California San Francisco, San Francisco, CA.

<sup>3</sup> To whom correspondence should be addressed. Tel.: 31-30-2532328; Fax: 31-30-2532837; E-mail: a.akhmanova@uu.nl.

<sup>4</sup> The abbreviations used are: MKLP1, mitotic kinesin-like protein 1; bioGFP, a GFP tag with an N terminally attached peptide that can be biotinylated; DSSO, disuccinimidyl sulfoxide; CRK, citron kinase; gRNAs, guide RNAs.

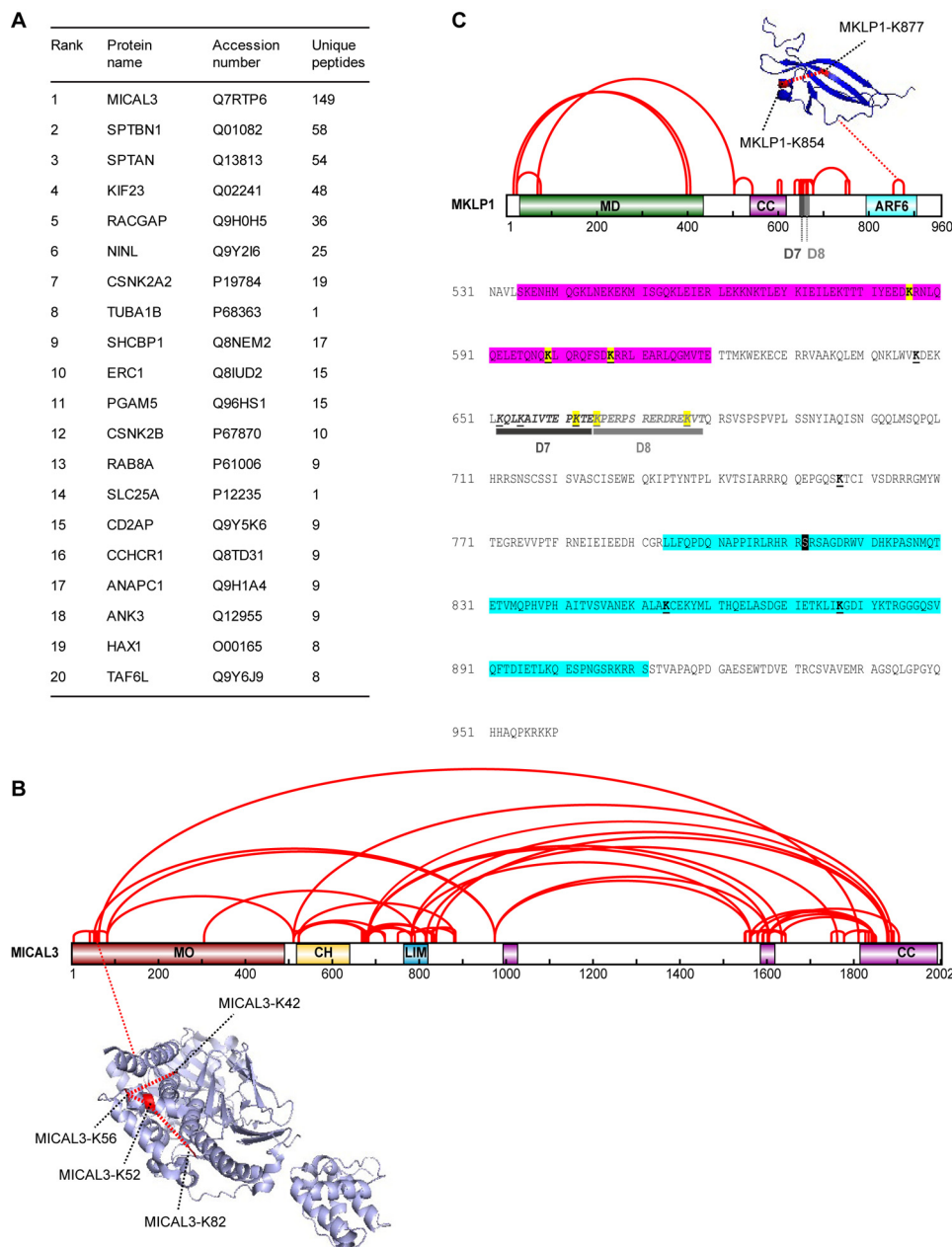


**FIGURE 1. Cross-linking mass spectrometry analysis of MICAL3-MKLP1 complex.** *A*, mass spectrometry-based analysis of the streptavidin pull-down assay with extracts of HEK293T cells expressing bioGFP-MICAL3 and BirA. *B*, schematic map of intraprotein cross-links in MICAL3 (red lines). Abbreviations for protein domains: MO, monooxygenase domain; CH, calponin homology domain; LIM, Lin11, Isl-1, and Mec-3 domain (zinc binding); CC, predicted coiled-coil. The cross-links identified within the MO domain, which are labeled with red dashed lines, were mapped onto mouse MICAL1 monooxygenase structure (PDB code 4TXI). The cross-links are within the DSS maximal distance constraint of 28.4 Å. *C*, schematic map of intraprotein cross-links MKLP1 (red lines). Abbreviations for protein domains: MD, kinesin motor domain; D7, amino acids deleted in the D7 mutant; D8, amino acids deleted in the D8 mutant; ARF6, ARF6-binding region. The cross-link identified within the ARF6-binding domain, which is labeled with red dashed line, was mapped onto the mouse ARF6-MKLP1 complex structure (PDB code 3VHX). The cross-link is within the DSS maximal distance constraint of 28.4 Å. The amino acids sequence 531–960 of MKLP1 is shown. CC is highlighted in purple (535–620). The ARF6-binding region is highlighted in blue (794–911). Cross-linked lysines with MICAL3 are highlighted in yellow. The underlined lysines indicate intraprotein cross-links. D7 and D8 deletions are underlined in black and gray, respectively. Aurora B phosphorylation site (Ser-812) is indicated by a black box.

and that it acts in this process not as an actin disassembly factor but as a protein-binding hub.

## Results

*MICAL3 Interacts with MKLP1*—To get insight into the function of MICAL3, we performed a mass spectrometry-based screen for its binding partners. We co-expressed in HEK293T cells the biotin ligase BirA together with MICAL3

carrying a bioGFP tag, which consists of GFP with an N terminally attached artificial peptide that can be efficiently biotinylated by BirA (20), and performed streptavidin pull-down assays from the lysates of these cells. BioGFP alone was used as a negative control. MICAL3 was the highest specific hit in this experiment, and the already known partners of MICAL3, ELKS (ERC1) and Rab8A, were also identified with high confidence (Fig. 1A). We also identified  $\alpha$ - and  $\beta$ -spec-

trins (SPTAN and SPTBN1; Fig. 1A), which are large cortical proteins involved in the control of mechanical stability of cellular membranes and assembly of cortical cytoskeleton and specialized membrane domains (21–23). Because MICAL3 can regulate actin disassembly, its binding to spectrins might play a role in controlling the organization of the cortical actin networks.

Among the other major hits in this screen were the two components of the centralspindlin complex, MKLP1 (KIF23) and CYK-4 (RACGAP) (Fig. 1A). The validity of the interaction with centralspindlin is supported by the fact that MICAL3 was previously reported as one of the potential partners of MKLP1 in HeLa cells in a high-throughput screen (24).

To investigate the interaction between MICAL3 and MKLP1 in more detail, we performed cross-linking mass spectrometry experiments. BioGFP-MICAL3 was co-expressed in HEK293 cells together with GFP-MKLP1 and BirA, biotinylated proteins were isolated by streptavidin pulldown, cross-linked on beads using disuccinimidyl sulfoxide (DSSO), and the cross-linked peptides were analyzed by mass spectrometry as described previously (25). We identified multiple cross-links within both MICAL3 and MKLP1. The cross-links within folded domains of known structure (MICAL1 monooxygenase, MKLP1 C terminus) were in good agreement with the DSSO distance constraint of 28.4 Å (23.4 Å for the maximal distance constraint of the DSSO cross-linker plus 5-Å tolerance for protein flexibility in solution), validating our cross-linking mass spectrometry approach (Fig. 1, B and C, and [supplemental Table S1](#)). We also found many cross-links between different domains of MICAL3, compatible with the previously proposed autoinhibitory folding of MICAL proteins (Fig. 1B and [supplemental Table S1](#)) (8, 26).

Specific cross-links were also observed between the second and third coiled-coil region of MICAL3 and the coiled-coil and the adjacent C-terminal domain of MKLP1 (Figs. 1C and 2A, and [supplemental Table S1](#)). Pulldown assays confirmed the cross-linking results and showed that the minimal MKLP1-binding domain of MICAL3 encompasses its C-terminal coiled-coil region (MICAL3-CC4), whereas a stronger interaction was observed with a larger C-terminal fragment, which includes all the cross-linked sites (MICAL3-CC3, Fig. 2, B–E). Because the C termini of MICAL1 and MICAL3 are quite similar, we have also tested whether MICAL1 can interact with MKLP1, but found that this was not the case (Fig. 2D).

The minimal MICAL3-binding domain of MKLP1 was present in the strongly charged and likely unstructured region located at the C-terminal side of the coiled coil of MKLP1 (Figs. 2A and 3, A–C). By deletion mapping, we identified a region of 13 residues, which was essential for the interaction (mutant D7), whereas the deletion of the adjacent 15-amino acid region (mutant D8) did not perturb the binding (Figs. 1C and 3, A and D, and [supplemental Table S1](#)). Taken together, our results show that MKLP1 and MICAL3 primarily interact through the unstructured polypeptide region in MKLP1 and the C-terminal coiled-coil domain of MICAL3, with additional contacts provided by the second coiled-coil domain of MICAL3 and the coiled-coil domain of MKLP1.

*MKLP1 Recruits MICAL3 to the Central Spindle and the Midbody*—We next examined the localization of endogenous MICAL3 in mitotic cells and found that whereas no conspicuous localization of MICAL3 could be detected at the early cell division stages, MICAL3 was clearly enriched at the spindle midzone starting from anaphase and strongly accumulated at the central spindle and the midbody during cytokinesis (Fig. 4A). Fluorescently tagged MICAL3 colocalized with the endogenous MKLP1 at the central spindle and the midbody (Fig. 4B). This localization did not depend on the enzymatic activity of MICAL3 as it was observed with the enzymatically dead MICAL3 mutant (Fig. 4C). Importantly, in MKLP1-depleted cells, MICAL3 failed to localize to the spindle midzone, indicating that MKLP1 targets MICAL3 to this location (Fig. 4, D–G).

We next set out to test whether MICAL3 affects the localization of MKLP1. Because we did not manage to achieve an efficient siRNA-mediated knockdown of MICAL3, we used CRISPR/Cas9-mediated knock-out technology. Cells transfected with a vector co-expressing a puromycin resistance gene, a single guide RNA sequence specific for MICAL3 and Cas9 (27) were subjected to puromycin selection and analyzed at 6–7 days after transfection to avoid the selection of cells, in which the potential cell division defects would be compensated by secondary mutations. This procedure led to highly efficient knock-out of MICAL3 protein expression (Fig. 4H). We found that the loss of MICAL3 had no effect on MKLP1 binding to the central spindle or the midbody (Fig. 4I). We conclude that MICAL3 is recruited to sites of centralspindlin accumulation but has no effect on its distribution.

*MICAL3 Is Required for Cytokinesis*—To determine whether the loss of MICAL3 affects cell division, we performed phase-contrast-based live imaging experiments and found that compared with the cells transfected with the vector alone, MICAL3 knock-out cells displayed a slight delay between the mitotic onset and the initiation of furrow ingression, and a very significant (more than 2-fold) increase in the time between the completion of furrow ingression and abscission (Fig. 5, A–C, and [supplemental Movies S1 and S2](#)). We observed no abnormalities during the formation or ingression of the cleavage furrow and detected no visible defects in the organization of the actin cytoskeleton during different mitotic stages, including cytokinesis (Fig. 6, A and B). The data indicate that the actin-depolymerizing activity of MICAL3 is unlikely to contribute to the dynamics of the actomyosin ring. We did, however, observe a significant increase in the percentage of cells that fused back after furrow ingression and the corresponding increase in the percentage of binucleated cells (from ~2 to ~10%) (Fig. 5, A, D, and E, and [supplemental Movie S3](#)). To test whether this effect of MICAL3 was specific, we performed rescue experiments with GFP-tagged MICAL3 expression constructs (Fig. 5F). Although no rescue was observed with GFP alone, we could completely rescue the binucleated phenotype by either the full-length MICAL3 or its enzymatically dead mutant, but not with the MICAL3 deletion mutant lacking the MKLP1-binding C terminus (Fig. 5F). Thus, these data indicate that MICAL3 contributes to the stabilization and/or maturation of the intercellular bridge in a way that does not require its monooxygenase activity.



## MICAL3 in Cytokinesis

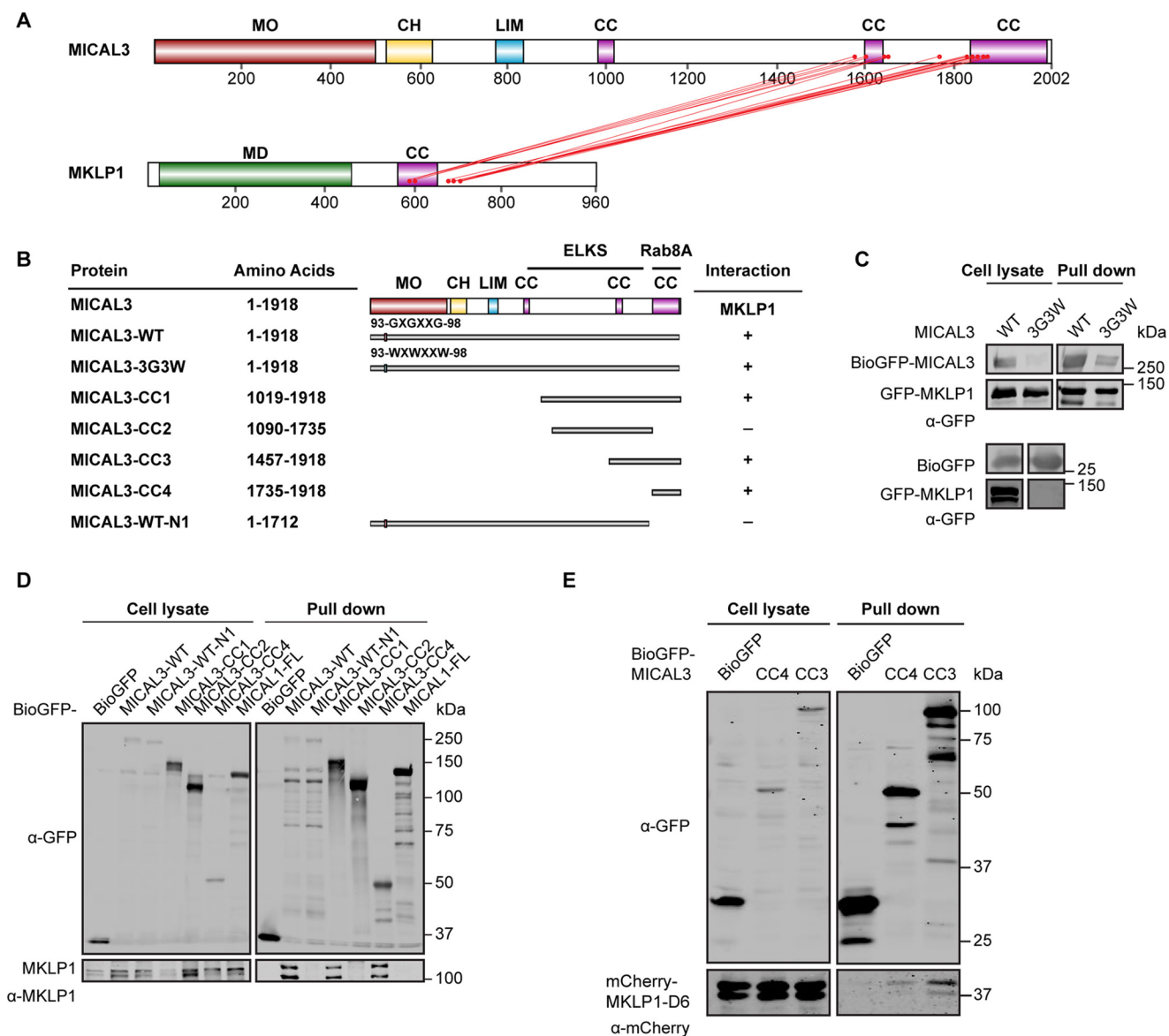


**FIGURE 2. Mapping of the domains in MICAL3 required for the interaction with MKLP1.** *A*, schematic map of the MICAL3-MKLP1 complex based on interprotein cross-links (red lines). *B*, schematic overview of MICAL3 deletion mutants used in this study and a summary of identified interactions. Numbering is based on MICAL3 isoform 1 (NP\_056056). Binding regions for the known partners of MICAL3 are indicated. *C–E*, streptavidin pull-down assays performed with the extracts of HEK293T cells co-expressing BirA, BioGFP, or the indicated MICAL3 or MKLP1 constructs. Antibodies against GFP, mCherry, or MKLP1 were used for Western blotting, as indicated.

For comparison, we examined the phenotype of MKLP1 depletion and found that, as expected, its effect on cytokinesis was much more profound than that of MICAL3 knock-out, with ~70% of binucleated cells (Fig. 5G). We observed a very significant although not complete rescue of this phenotype by expressing GFP-MKLP1 (Fig. 5G). The MKLP1 deletion mutant D7, which was unable to bind to MICAL3 and promote MICAL3 localization to the midbody (Figs. 3D and 5H), performed significantly less well in the rescue experiments than the wild type MKLP1 and the MKLP1-D8 mutant, which could restore MICAL3 accumulation at the midbody in MKLP1-depleted cells (Fig. 5, G and H). Although we cannot exclude that the D7 mutant perturbs MKLP1 function in ways unrelated to MICAL3 binding, our results are fully compatible with a role of MKLP1-dependent

recruitment of MICAL3 as a factor contributing to the successful completion of cytokinesis.

*MICAL3 Promotes the Recruitment of ELKS and Rab8 to the Intercellular Bridge*—Because our data indicated that the contribution of MICAL3 to cytokinesis does not require its actin-destabilizing monooxygenase activity, we turned our attention to its binding partners. We first examined the distribution of ELKS, which was shown previously to bind to MICAL3 and participate in secretory vesicle docking (8). We found that ELKS prominently localized to the midbody in 90% of the cells, and that this localization was completely lost in MICAL3 knock-out cells (Fig. 7, A and B). Because MICAL3 is targeted to the midbody by MKLP1, these results suggest that MICAL3 might be able to connect ELKS to MKLP1. In support of this, mass spectrometry-based analysis of BioGFP-ELKS pull downs

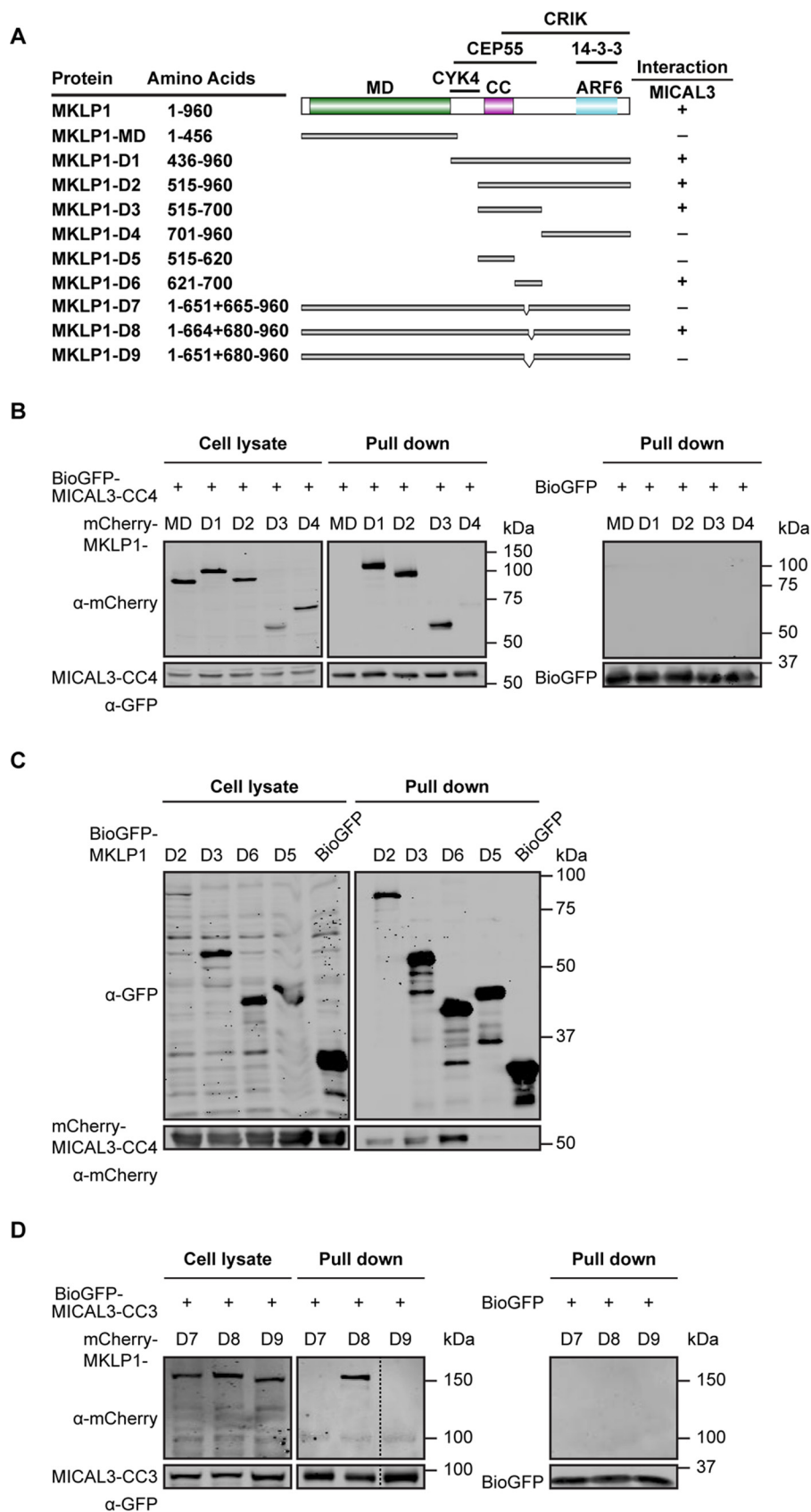
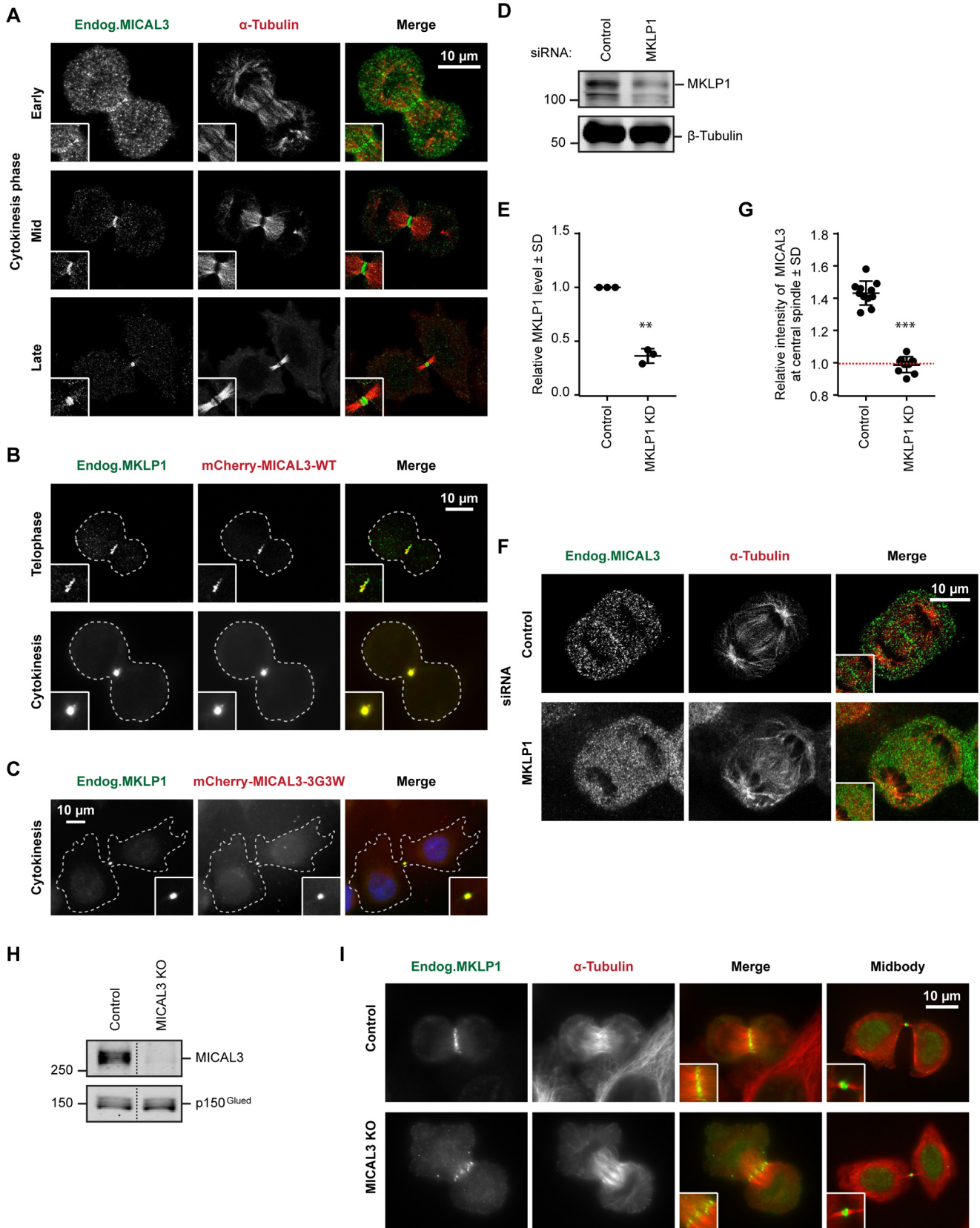


FIGURE 3. **Mapping of the domains in MKLP1 required for the interaction with MICAL3.** A, schematic overview of MKLP1 deletion mutants used in this study and a summary of identified interactions. Numbering is based on MKLP1 isoform 1 (NCBI protein NP\_612565). Binding regions for the known partners of MKLP1 are indicated. B–D, streptavidin pull-down assays performed with the extracts of HEK293T cells co-expressing BirA, BioGFP, or the indicated MICAL3 or MKLP1 constructs. Antibodies against GFP or mCherry were used for Western blotting, as indicated. An empty lane cropped in D is indicated by a dashed line.

## MICAL3 in Cytokinesis

from HEK293 cells identified MKLP1 (KIF23) as a potential interacting partner (Fig. 7C). We next tested whether the interaction between MKLP1 and ELKS is mediated by MICAL3 and found

that co-expression of MICAL3 indeed enhanced the ability of MKLP1 to co-precipitate ELKS (Fig. 7D). We conclude that MICAL3 can form a triple complex with MKLP1 and ELKS and





through the interaction with the former, target the latter to the midbody.

We have also examined the distribution of Rab8A-labeled membranes. Rab8A was present at ~75% of the midbodies (Fig. 8, *A* and *B*). The intercellular bridges lacking Rab8A-positive structures appeared to represent very late stages of cytokinesis, in line with previous publications showing that Rab8A-positive vesicles are removed from the intercellular bridge prior to abscission (13, 14). The percentage of cells that exhibited at least some Rab8A signal at the intercellular bridge was significantly reduced in MICAL3 knock-out cells (Fig. 8, *A* and *B*), and the intensity of Rab8A staining in the midbody region was also reduced (Fig. 8*C*). In contrast, the localization of transferrin receptor-positive or Rab11-positive endosomes to the midbody was not perturbed by MICAL3 knock-out (Fig. 8, *D* and *E*). We conclude that MICAL3 specifically contributes to the recruitment of Rab8A to the midbody.

Mass spectrometry-based analysis of ELKS binding partners in HEK293 cells identified citron kinase (CRIK) and its binding partner kinesin-3 KIF14 (Fig. 7*C*), whereas these proteins were not present in the MICAL3 pull down (Figs. 1*A* and 7*C*). We have examined whether the localization of CRIK or KIF14 was perturbed in MICAL3 knock-out cells and found this not to be the case (Fig. 8*F*). Although these data do not rule out that ELKS, localized to the midbody through its interaction with MICAL3, somehow affects the function of CRIK-containing protein complexes, they indicate that MICAL3 does not participate in the targeting of this signaling protein complex to the intercellular bridge, in line with the data showing that CRIK directly interacts with MKLP1 (28).

**ELKS and Rab8A Are Required for Cytokinesis**—If the cytokinetic defect of MICAL3 knock-out cells occurs due to the inability to properly localize ELKS and Rab8A-positive membranes, then the depletion of these proteins can be expected to perturb cytokinesis as well. We examined this possibility by depleting ELKS and knocking down ELKS and Rab8A (Fig. 8, *G* and *H*); the two proteins were depleted by 75% and 95%, respectively. The intensity of Rab8A staining in the midbody region in ELKS-depleted cells was reduced to values close to background (Fig. 8, *A* and *I*). The depletion of either ELKS or Rab8A led to a significant increase of binucleated cells (~10%, similar to MICAL3 knock-out) (Fig. 8, *J* and *K*). We conclude that the complex of MICAL3 and ELKS helps to target Rab8A to the intercellular bridge, and that all three proteins are required to the proper maturation of the bridge, which prevents the bridge recession and promotes timely abscission.

## Discussion

In this study we identified MICAL3 as a new molecular player in cytokinesis and a binding partner of MKLP1. Previous work

has shown that centralspindlin represents a major binding hub for different factors involved in cytokinesis (4), and our current work added MICAL3 to the list of MKLP1 interactors. Cross-linking experiments combined with mass spectrometry allowed us to show that the MICAL3-MKLP1 association is direct and to characterize the contact sites between the two proteins, illustrating the power of this approach. The MICAL3-binding region of MKLP1 is distinct from the MKLP1 sites known to bind to CYK-4, ARF6, or 14-3-3, but there might be some overlap with the binding sites for CRIK and CEP55 (Fig. 3*A*) (28–32). The MKLP1 binding site of MICAL3 overlaps with that of Rab8A but is different from the region involved in the interaction with ELKS (8) (Fig. 2*B*), and in agreement with these data, we showed that MICAL3 can connect ELKS to MKLP1.

Our data indicate that MICAL3 is involved in stabilization and maturation of the intercellular bridge, because its loss led to increased frequency of cytokinetic failure and extended duration of abscission. Surprisingly, despite the well established role of MICAL enzymes in actin disassembly, we found no evidence that MICAL3 regulates actin cytoskeleton during cytokinesis. Instead, MICAL3 recruits ELKS and Rab8A to the midbody (Fig. 9), and the depletion of these two proteins caused an increase of binucleated cells, indicative of cytokinetic defect. The function of MICAL3 in cytokinesis thus appears to be mechanistically similar to that of the MICAL3-related protein MICAL-L1, which lacks an enzymatic domain, localizes to the midbody, and plays a role in organizing recycling endosomes at the intercellular bridge (33).

The next challenge is to identify the exact molecular role of Rab8A vesicles in cytokinesis. Because these vesicles are cleared from the intercellular bridge before the actual abscission (13–14), we favor the idea that they transport molecules required for the maturation of the intercellular bridge and the midbody, such as some signaling factors. This function would be similar to that of Rab35, which contributes to actin depolymerization by delivering to the intercellular bridge the phosphoinositide phosphatase OCRL (34, 35). The role of Rab8A vesicles in protein delivery to the midbody would be consistent with the observation that the enzymatic activity of MICAL3 is not essential for the cytokinetic function despite the fact that it promotes vesicle fusion with the plasma membrane.

The loss of MICAL3, ELKS, and Rab8A caused a similar, relatively mild cytokinetic defect, with ~10% binucleated cells, indicating that the absence of these proteins can be compensated by other factors, at least in HeLa cells, although the situation might be different in other systems. It is possible that different vesicular populations at the midbody have partially overlapping functions. Although Rab8A can be recruited to Rab11-positive recycling endosomes (11), the MICAL3-depen-

**FIGURE 4. MKLP1 recruits MICAL3 to the central spindle and the midbody.** *A–C*, localization of endogenous MICAL3 (*A*, green), mCherry-MICAL3-WT (*B*, red), or mCherry-MICAL3-3G3W (*C*, red) during cytokinesis. HeLa cells were stained with the indicated antibodies. Cell outlines are indicated by dashed lines. *Insets*, magnifications of the boxed areas. *D* and *E*, Western blots (*D*) and quantification of normalized immunoblot values (*E*) for MKLP1 expression in HeLa cells 72 h after transfection with the control (luciferase) or MKLP1 siRNAs. \*\*,  $p < 0.01$ , Student's *t* test based on 3 independent experiments. *F* and *I*, immunostaining of MICAL3 (*F*) or MKLP1 (*I*) (green) and  $\alpha$ -tubulin (red) in HeLa cells 72 h after transfection with the indicated siRNAs. *Insets*, magnifications of the boxed areas. *G*, relative intensity of MICAL3 at the central spindle compared with cytoplasm in control and MKLP1 knockdown cells. The red dashed line indicates the background level, equal to 1. \*\*\*,  $p < 0.001$ , Mann-Whitney *U* test. More than 20 cells analyzed from 3 independent experiments. *H*, Western blots of extracts of control and MICAL3 knock-out HeLa cells. Additional samples present on the gel were cropped as indicated by a dashed line.

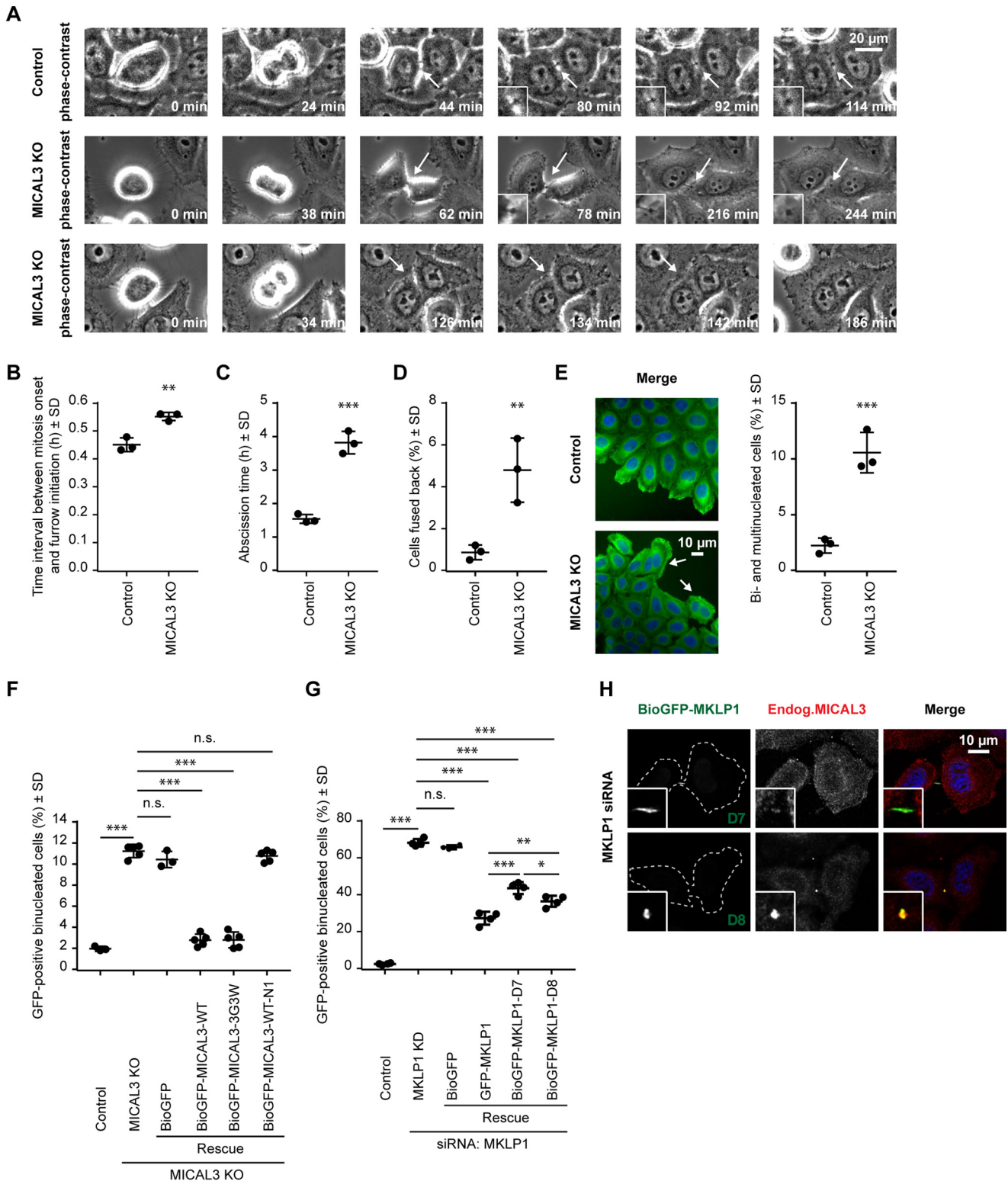


FIGURE 5. Cytokinesis defects in MICAL3 knock-out cells. *A*, phase-contrast-based live imaging of control and MICAL3 knock-out cells. *Insets* show magnifications of intercellular bridges or cell membrane (*arrows*). See also *supplemental Movies S1–S3*. *B–D*, time interval between mitosis onset and furrow initiation (*B*), abscission time (*C*), and percentage of the cells fused back without completing cytokinesis (*D*) in control and MICAL3 knock-out cells. Data represent more than 150 cells from 3 independent experiments, \*\*,  $p < 0.01$ ; \*\*\*,  $p < 0.001$ , Student's *t* test. *E*, immunostaining of  $\alpha$ -tubulin (*green*) and DAPI (*blue*) in control or MICAL3 knock-out cells, with binucleated cells indicated with *white arrows*, and quantification of the percentage of bi- and multinucleated cells in control and MICAL3 knock-out cells. Data represent more than 1000 cells from 3 independent experiments, \*\*\*,  $p < 0.001$ , Student's *t* test. *F* and *G*, percentage of binucleated cells determined by counting GFP-positive cells in rescue experiments of MICAL3 knock-out (*F*) or MKLP1 knockdown (*G*) with the indicated constructs. Data represent more than 3000 cells from 4 or 5 independent experiments, \*,  $p < 0.05$ ; \*\*,  $p < 0.01$ ; \*\*\*,  $p < 0.001$ , *n.s.*,  $p > 0.05$ , Student's *t* test. *H*, immunostaining of BioGFP-MKLP1-D7/D8 (*green*) and MICAL3 (*red*) in MKLP1 knockdown cells. Cell outlines are indicated by *dashed lines*. Magnified midbody images are shown in *insets*.



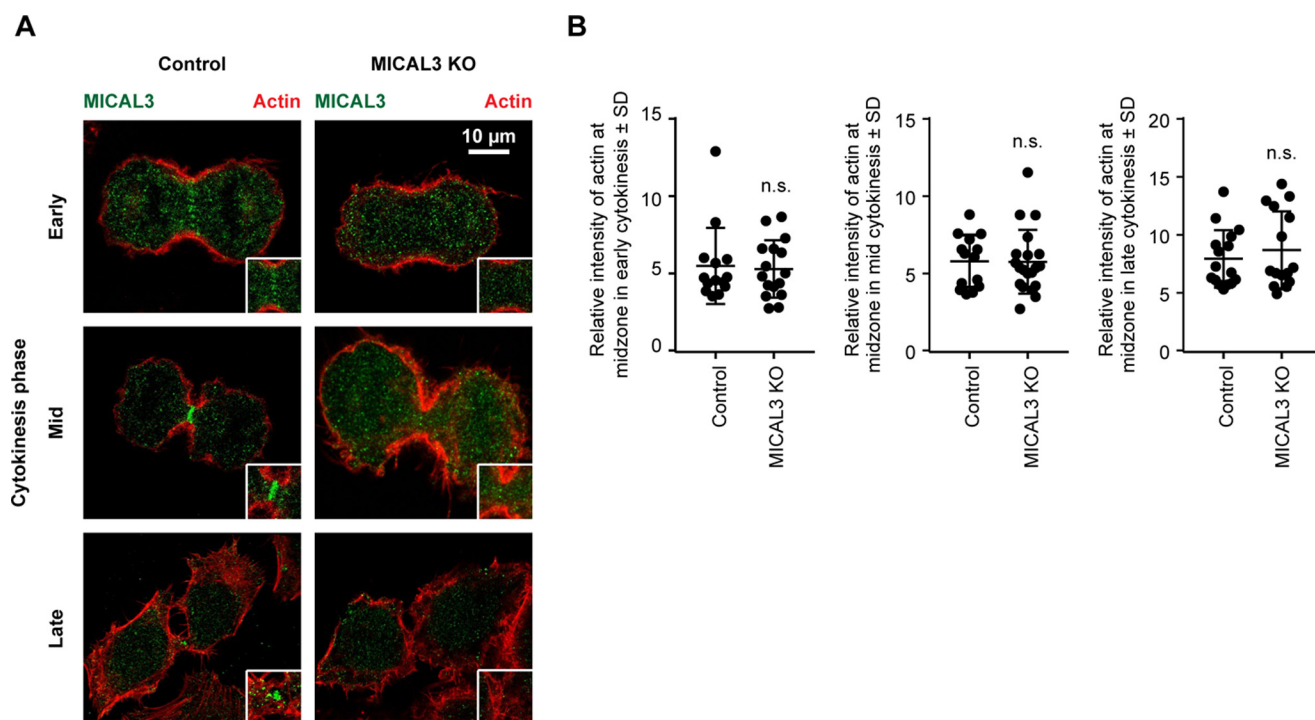


FIGURE 6. **Actin distribution in MICAL3 knock-out cells.** *A*, immunostaining of MICAL3 (green) and actin (red) in control or MICAL3 knock-out cells. *Insets*, magnifications of the boxed areas. *B*, ratio of the intensity of actin at midzone to intensity in the cytoplasm in control or MICAL3 knock-out cells at different stages of cytokinesis. Around 100 cells were analyzed in 3 independent experiments. *n.s.*,  $p > 0.05$ , Mann-Whitney *U* test.

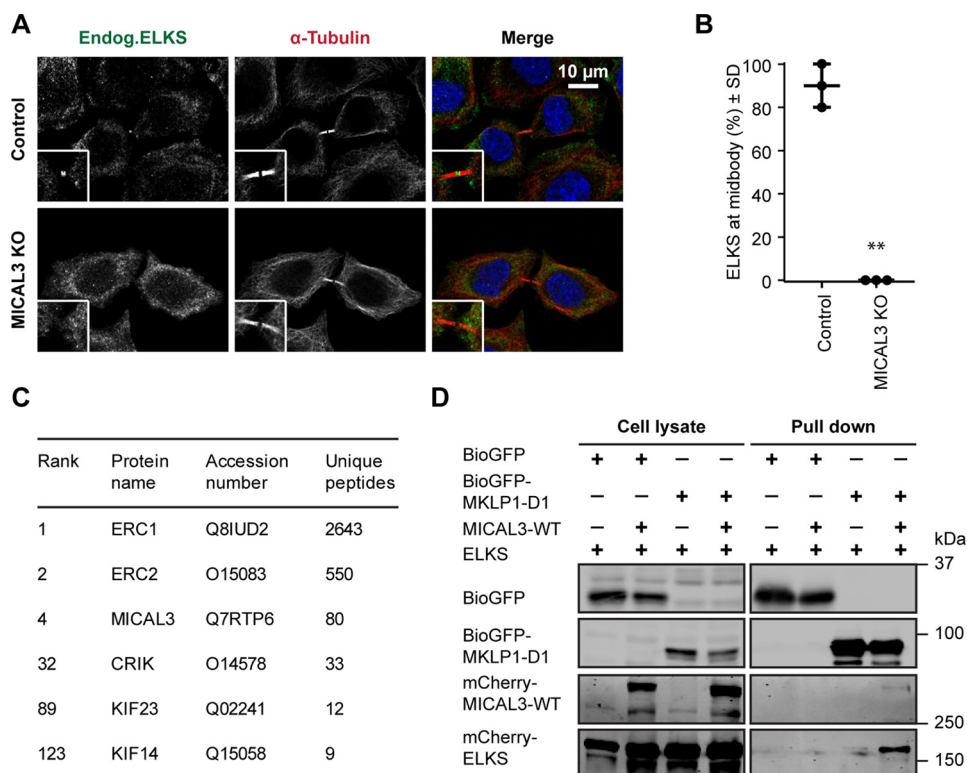
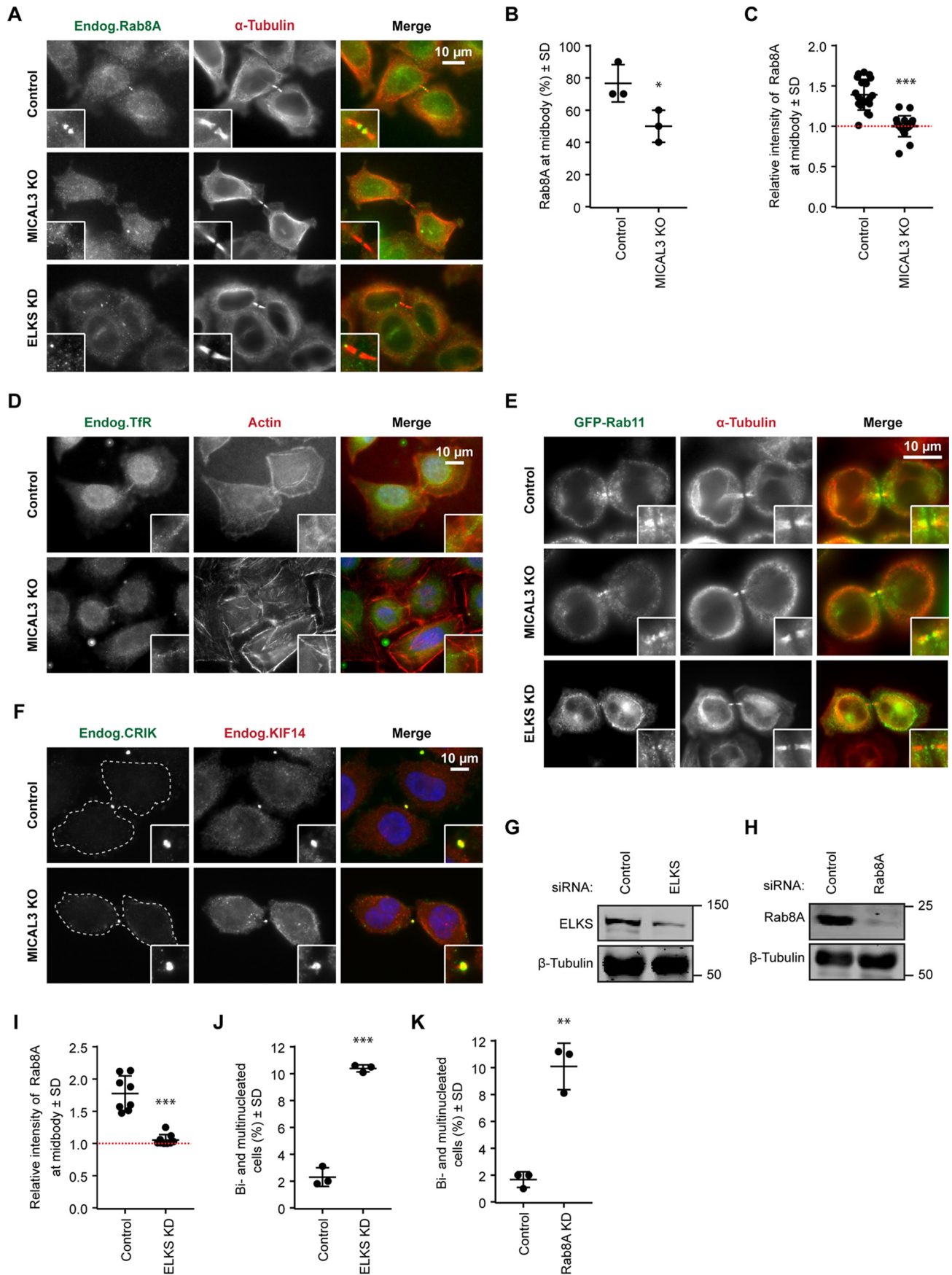


FIGURE 7. **MICAL3 is required for ELKS localization to the midbody.** *A*, immunostaining of ELKS (green) and  $\alpha$ -tubulin (red) in control or MICAL3 knock-out cells. *Insets*, magnified midbody images. *B*, percentage of cells with detectable specific ELKS staining at the midbody in control and MICAL3 knock-out cells. Data represent 60 cells from 3 independent experiments. \*\*,  $p < 0.01$ , Student's *t* test. *C*, mass spectrometry-based analysis of streptavidin pull-down assay with the extracts of HEK293T cells expressing biotinylation-tagged ELKS and BirA. *D*, streptavidin pull-down assays performed with the extracts of HEK293T cells co-expressing BirA and the indicated proteins, analyzed by Western blotting with antibodies against GFP or mCherry.



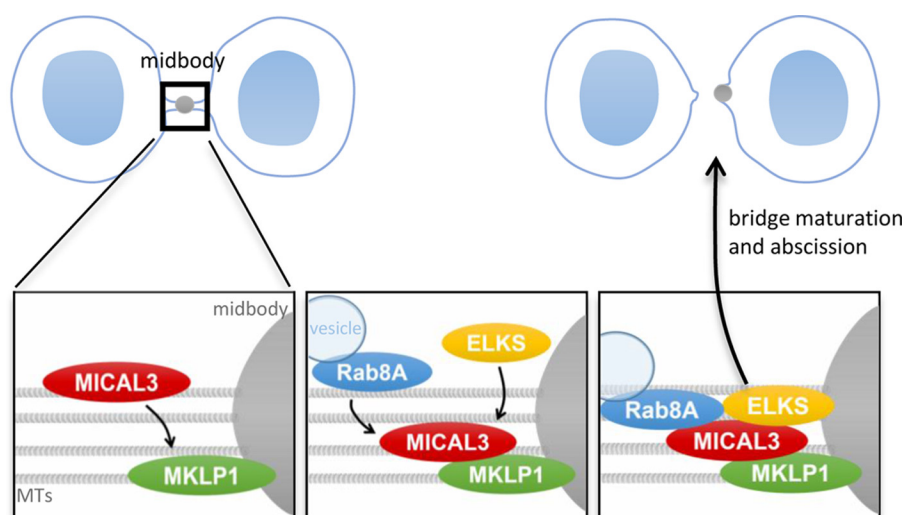


FIGURE 9. **A model for MICAL3 function during cytokinesis.** Schematic representation of the model described in this study. MKLP1 localizes to the midbody and recruits MICAL3, which in turn participates in recruiting ELKS and Rab8A-bound vesicles. As a complex, they promote maturation of the intercellular bridge and abscission.

dent population of Rab8A vesicles at the midbody is distinct from Rab11-labeled endosomes, which were not affected by MICAL3 knock-out. The Rab8A vesicles studied here might overlap with the post-Golgi carriers, which were previously described to participate in cytokinesis (36, 37). Golgi-dependent secretory trafficking was shown to be necessary for cytokinesis during development in invertebrates (5, 7), and a similar function might be also important in mammals, constituting a potentially interesting avenue for future studies.

## Experimental Procedures

### DNA Constructs and siRNAs

We used the following previously described constructs: BioGFP-MICAL3-WT, mCherry-MICAL3-WT, BioGFP-MICAL3-3G3W, and mCherry-MICAL3-3G3W (8). Deletion mutants of MICAL3 were cloned by PCR-based strategy. GFP-MKLP1 constructs were based on plasmids that were a gift from Dr. Stephen Doxsey (University of Massachusetts) and M. Mishima (Warwick Medical School, UK). BioGFP-MICAL1-FL was a gift from Dr. R. J. Pasterkamp (UMC Utrecht, The Netherlands). GFP-Rab11 was purchased from Addgene, Cambridge, MA (plasmid number 12674).

The target sequences of control and ELKS siRNAs were described previously (38). MKLP1 siRNA was described in Ref. 39. MICAL1 siRNA was synthesized by Ambion (ID s230028). Rab8A siRNA corresponded to the target sequence GGAAAGCACAAATGAAGGA. Cells were transfected with 10 nM siRNAs using HiPerFect (Qiagen) and analyzed 3 days after transfection.

### Cell Culture and CRISPR/Cas9-mediated Knockouts

HEK293T and HeLa were cultured as described previously (8). We used FuGENE 6 (Promega) for plasmid transfection, and HiPerFect (Qiagen) for siRNA transfection of HeLa cells; polyethylenimine (Polysciences) was used to transfect HEK293T cells for streptavidin pulldown assays, which were performed as described previously (8).

The target sequence for CRISPR targeting the human MICAL3 gene was CCCAGTAAGGATAAGTCGA (Exon 3). Two complementary oligonucleotides with BpiI restriction sites for guide RNAs (gRNAs) were synthesized, and cloned into pX459 CRISPR/Cas9-Puro vector (27) (Addgene). HeLa cells were transfected with pX459 vector or pX459-MICAL3 gRNA and treated with 2  $\mu$ g/ml of puromycin for 2 days and analyzed within a 4-day period post-puromycin treatment.

### Antibodies and Immunofluorescence Cell Staining

We used homemade rabbit polyclonal antibodies against MICAL3, MKLP1 (Santa Cruz Biotechnology), GFP (Abcam, ab290), ELKS (Proteintech, 22211-1-AP), KIF14 (Bethyl Laboratories), and Rab8A (a gift of J. Peränen, University of Helsinki, Finland) (40). We used mouse monoclonal antibodies against mCherry (Clontech, 632543),  $\beta$ -tubulin (Sigma, T5201), p150<sup>Glued</sup> (BD Biosciences, 610474), actin (Chemicon), CRIK (BD Biosciences), transferrin receptor (Roche Applied Science), and rat monoclonal antibodies against  $\alpha$ -tubulin YL1/2 (Pierce, MA1-80017). The following secondary antibodies were used: IRDye 800CW/680LT goat anti-rabbit and anti-mouse (Li-Cor Biosciences); Alexa 488- and Alexa 594-conju-

FIGURE 8. **MICAL3, Rab8A, and ELKS act in the same cytokinesis pathway.** A and D–F, immunostaining of Rab8A (A), transferrin receptor (*TfR*) (D), GFP-Rab11 (E), or CRIK (F) (green) and  $\alpha$ -tubulin (A and E), actin (D), or KIF14 (F) (red) in control or the indicated knock-out or knockdown cells. Cell outlines are indicated by dashed lines. Insets, magnified midbody images. B, percentage of cells with detectable specific Rab8A staining at the midbody in control and MICAL3 knock-out cells. Data represent 60 cells from 3 independent experiments. \*,  $p < 0.05$ , Student's *t* test. C and I, relative intensity of Rab8A at the midbody compared with cytoplasm in the indicated control, knock-out, or knockdown cells. The red dashed line indicates background level, equal to 1. 15 to 40 cells were analyzed in 3 independent experiments. \*\*\*,  $p < 0.001$ , Mann-Whitney *U* test. G and H, Western blots of extracts of HeLa cells after 72 h of transfection with the indicated siRNAs. J and K, percentage of bi- and multinucleated cells after transfection with the indicated siRNAs. Data represent more than 2000 cells from 3 independent experiments; \*\*,  $p < 0.01$ ; \*\*\*,  $p < 0.001$ , Student's *t* test.



## MICAL3 in Cytokinesis

gated goat antibodies against rabbit, rat, and mouse IgG (Molecular Probes). The Alexa 594-conjugated phalloidin were purchased from Invitrogen.

To label proteins, cells were fixed with  $-20^{\circ}\text{C}$  methanol for 10 min or 3.7% paraformaldehyde in PBS for 10 min at room temperature. Cells were permeabilized with 0.1% Triton X-100 in phosphate-buffered saline (PBS) for 10 min; subsequent washing and labeling steps were carried out in PBS supplemented with 2% bovine serum albumin and 0.05% Tween-20. At the end, slides were rinsed in 70 and 100% ethanol or air-dried and mounted in Vectashield mounting medium (Vector Laboratories).

### Mass Spectrometry

**Sample Preparation**—Samples were prepared from pulldown assays of biotinylated proteins from extracts of transfected HEK293T cells using streptavidin beads, and analyzed by subsequent mass spectrometry experiments as described previously (8). For the cross-linking experiment, the immunoprecipitated proteins were on-beads cross-linked using 1 mM DSSO cross-linker (41). The cross-linking reaction was carried out for 1 h at room temperature and quenched with 20 mM Tris-HCl (pH 7.8) for 30 min at room temperature. Subsequently, the on-beads cross-linked proteins were denatured with 2 mM urea, reduced with 4 mM dithiothreitol at  $56^{\circ}\text{C}$  for 30 min and alkylated with 8 mM iodoacetamide at room temperature for 30 min in the dark. Proteins were digested using trypsin at an enzyme-to-protein ratio of 1:20 (w/w) at  $37^{\circ}\text{C}$  for 2 h. The supernatant was removed from the beads and further digested at  $37^{\circ}\text{C}$  overnight. Protein digests were desalted using Sep-Pak  $\text{C}_{18}$  cartridges (Waters), dried, and stored at  $-20^{\circ}\text{C}$  for further use. The desalted digests were SCX fractionated as previously described (25), and only the late SCX fractions (predominantly containing higher charged species) were subjected to LC/MS analysis.

**LC/MS/MS Analysis**—Peptides and cross-linked peptides were analyzed using an ultra HPLC Proxeon EASY-nLC 1000 system (Thermo Fisher Scientific) coupled on-line to an ETD enabled LTQ Orbitrap Elite mass spectrometer (Thermo Fisher Scientific). For cross-link analysis, reversed-phase separation and MS data acquisition were performed as previously described and data analysis was accomplished using XlinkX software (25). Results were filtered by 1% false discovery rate and all reported cross-links were manually validated. For peptide identification, rapid CID was used for data acquisition. Peptide identification was performed using Proteome Discoverer 1.4 (Thermo Fisher Scientific). Results were filtered by 1% false discovery rate.

### Image Acquisition

Images of fixed cells were collected with a Nikon Eclipse 80i upright fluorescence microscope and a CoolSNAP HQ2 CCD camera (Photometrics), using a Nikon Plan Apo VC  $\times 60/\text{N.A.}1.40$  oil objective or Nikon Plan Apo VC  $\times 100/\text{N.A.}1.40$   $\times$  oil objective.

Live-cell phase-contrast imaging was performed on inverted research microscope Nikon Eclipse Ti-E (Nikon) with the perfect focus system (Nikon), equipped with a Nikon Plan Apo

chromat  $\times 20/0.75$  phase-contrast objective (Nikon), a CoolSNAP HQ2 CCD camera (Photometrics), and controlled with Micro-Manager Open Source Microscopy Software. To keep the cells at  $37^{\circ}\text{C}$ , a stage top incubator model INUBG2E-ZILCS (Tokai Hit) was used. Images were projected onto the CCD chip at a magnification of  $0.3215\ \mu\text{m}/\text{pixel}$ . Round 25-mm coverslips were mounted in Attofluor Cell Chamber (Thermo Fisher) and maintained at  $37^{\circ}\text{C}$  and 5%  $\text{CO}_2$ . Cells were imaged every 2 min for 6–12 h.

Confocal 300-nm Z-stack images were acquired on a Leica SP8 DMI STED microscope equipped with a  $\times 100$  HC PI Apo objective (Leica, NA 1.4. oil) and the Leica HyD detector controlled by the Leica Application Software X. Excitation of Alexa 488, Alexa 568, and Alexa 647 was performed with a SuperK EXTREME supercontinuum laser (NKT photonics) and DAPI was excited using a 405-nm diode laser controlled by a PDL800-B module (PicoQuant). Channels were imaged sequentially with a pixel size between 90 and 110 nm. Presented images are projections of 6–10 Z-planes, processed in ImageJ.

**Author Contributions**—A. A. conceived and coordinated the study and wrote the paper. Q. L., F. L., K. L. Y., and A. S.-M. designed, performed, and analyzed the experiments. L. C. K. and A. J. R. H. contributed to the coordination of the study, data analysis and writing the paper. R. T., I. G., and S. R. provided technical assistance with the experiments and their analysis and contributed to the preparation of the figures. All authors reviewed the results and approved the final version of the manuscript.

**Acknowledgments**—We thank S. Doxsey, M. Mishima, J. Peränen, and J. Pasterkamp for the gift of materials, and Dr. J. Demmers (Erasmus MC, Rotterdam) for the help with mass spectrometry experiments.

### References

1. Mierzwa, B., and Gerlich, D. W. (2014) Cytokinetic abscission: molecular mechanisms and temporal control. *Dev. Cell* **31**, 525–538
2. Green, R. A., Paluch, E., and Oegema, K. (2012) Cytokinesis in animal cells. *Annu. Rev. Cell Dev. Biol.* **28**, 29–58
3. Glotzer, M. (2009) The 3Ms of central spindle assembly: microtubules, motors and MAPs. *Nat. Rev. Mol. Cell Biol.* **10**, 9–20
4. White, E. A., and Glotzer, M. (2012) Centralspindlin: at the heart of cytokinesis. *Cytoskeleton* **69**, 882–892
5. Schiel, J. A., and Prekeris, R. (2013) Membrane dynamics during cytokinesis. *Curr. Opin. Cell Biol.* **25**, 92–98
6. Gould, G. W. (2016) Animal cell cytokinesis: the role of dynamic changes in the plasma membrane proteome and lipidome. *Semin. Cell Dev. Biol.* **53**, 64–73
7. Albertson, R., Riggs, B., and Sullivan, W. (2005) Membrane traffic: a driving force in cytokinesis. *Trends Cell Biol.* **15**, 92–101
8. Grigoriev, I., Yu, K. L., Martinez-Sanchez, E., Serra-Marques, A., Smal, I., Meijering, E., Demmers, J., Peränen, J., Pasterkamp, R. J., van der Sluijs, P., Hoogenraad, C. C., and Akhmanova, A. (2011) Rab6, Rab8, and MICAL3 cooperate in controlling docking and fusion of exocytotic carriers. *Curr. Biol.* **21**, 967–974
9. Ang, A. L., Fölsch, H., Koivisto, U. M., Pypaert, M., and Mellman, I. (2003) The Rab8 GTPase selectively regulates AP-1B-dependent basolateral transport in polarized Madin-Darby canine kidney cells. *J. Cell Biol.* **163**, 339–350
10. Henry, L., and Sheff, D. R. (2008) Rab8 regulates basolateral secretory, but not recycling, traffic at the recycling endosome. *Mol. Biol. Cell* **19**, 2059–2068

11. Knödler, A., Feng, S., Zhang, J., Zhang, X., Das, A., Peränen, J., and Guo, W. (2010) Coordination of Rab8 and Rab11 in primary ciliogenesis. *Proc. Natl. Acad. Sci. U.S.A.* **107**, 6346–6351
12. Kaplan, A., and Reiner, O. (2011) Linking cytoplasmic dynein and transport of Rab8 vesicles to the midbody during cytokinesis by the doublecortin domain-containing 5 protein. *J. Cell Sci.* **124**, 3989–4000
13. Schiel, J. A., Simon, G. C., Zaharris, C., Weisz, J., Castle, D., Wu, C. C., and Prekeris, R. (2012) FIP3-endosome-dependent formation of the secondary ingression mediates ESCRT-III recruitment during cytokinesis. *Nat. Cell Biol.* **14**, 1068–1078
14. Guizetti, J., Schermelleh, L., Mäntler, J., Maar, S., Poser, I., Leonhardt, H., Müller-Reichert, T., and Gerlich, D. W. (2011) Cortical constriction during abscission involves helices of ESCRT-III-dependent filaments. *Science* **331**, 1616–1620
15. Hida, Y., and Ohtsuka, T. (2010) CAST and ELKS proteins: structural and functional determinants of the presynaptic active zone. *J. Biochem.* **148**, 131–137
16. Kolk, S. M., and Pasterkamp, R. J. (2007) MICAL flavoprotein monooxygenases: structure, function and role in semaphorin signaling. *Adv. Exp. Med. Biol.* **600**, 38–51
17. Terman, J. R., Mao, T., Pasterkamp, R. J., Yu, H. H., and Kolodkin, A. L. (2002) MICALs, a family of conserved flavoprotein oxidoreductases, function in plexin-mediated axonal repulsion. *Cell* **109**, 887–900
18. Giridharan, S. S., and Caplan, S. (2014) MICAL-family proteins: complex regulators of the actin cytoskeleton. *Antioxid. Redox Signal.* **20**, 2059–2073
19. Fukuda, M., Kanno, E., Ishibashi, K., and Itoh, T. (2008) Large scale screening for novel rab effectors reveals unexpected broad Rab binding specificity. *Mol. Cell. Proteomics* **7**, 1031–1042
20. de Boer, E., Rodriguez, P., Bonte, E., Krijgsveld, J., Katsantoni, E., Heck, A., Grosveld, F., and Strouboulis, J. (2003) Efficient biotinylation and single-step purification of tagged transcription factors in mammalian cells and transgenic mice. *Proc. Natl. Acad. Sci. U.S.A.* **100**, 7480–7485
21. Bennett, V., and Baines, A. J. (2001) Spectrin and ankyrin-based pathways: metazoan inventions for integrating cells into tissues. *Physiol. Rev.* **81**, 1353–1392
22. Baines, A. J. (2009) Evolution of spectrin function in cytoskeletal and membrane networks. *Biochem. Soc. Trans.* **37**, 796–803
23. Bennett, V., and Healy, J. (2009) Membrane domains based on ankyrin and spectrin associated with cell-cell interactions. *Cold Spring Harb. Perspect. Biol.* **1**, a003012
24. Maliga, Z., Junqueira, M., Toyoda, Y., Ettinger, A., Mora-Bermúdez, F., Klemm, R. W., Vasilj, A., Guhr, E., Ibarlucea-Benitez, I., Poser, I., Bonifacio, E., Huttner, W. B., Shevchenko, A., and Hyman, A. A. (2013) A genomic toolkit to investigate kinesin and myosin motor function in cells. *Nat. Cell Biol.* **15**, 325–334
25. Liu, F., Rijkers, D. T., Post, H., and Heck, A. J. (2015) Proteome-wide profiling of protein assemblies by cross-linking mass spectrometry. *Nat. Methods* **12**, 1179–1184
26. Schmidt, E. F., Shim, S. O., and Strittmatter, S. M. (2008) Release of MICAL autoinhibition by semaphorin-plexin signaling promotes interaction with collapsin response mediator protein. *J. Neurosci.* **28**, 2287–2297
27. Ran, F. A., Hsu, P. D., Wright, J., Agarwala, V., Scott, D. A., and Zhang, F. (2013) Genome engineering using the CRISPR-Cas9 system. *Nat. Protoc.* **8**, 2281–2308
28. Bassi, Z. I., Audusseau, M., Riparbelli, M. G., Callaini, G., and D'Avino, P. P. (2013) Citron kinase controls a molecular network required for midbody formation in cytokinesis. *Proc. Natl. Acad. Sci. U.S.A.* **110**, 9782–9787
29. Mishima, M., Kaitna, S., and Glotzer, M. (2002) Central spindle assembly and cytokinesis require a kinesin-like protein/RhoGAP complex with microtubule bundling activity. *Dev. Cell* **2**, 41–54
30. Makyio, H., Ohgi, M., Takei, T., Takahashi, S., Takatsu, H., Katoh, Y., Hanai, A., Ueda, T., Kanaho, Y., Xie, Y., Shin, H. W., Kamikubo, H., Kataoka, M., Kawasaki, M., Kato, R., Wakatsuki, S., and Nakayama, K. (2012) Structural basis for Arf6-MKLP1 complex formation on the Flemming body responsible for cytokinesis. *EMBO J.* **31**, 2590–2603
31. Joseph, N., Hutterer, A., Poser, I., and Mishima, M. (2012) ARF6 GTPase protects the post-mitotic midbody from 14-3-3-mediated disintegration. *EMBO J.* **31**, 2604–2614
32. Zhao, W. M., Seki, A., and Fang, G. (2006) Cep55, a microtubule-bundling protein, associates with centralspindlin to control the midbody integrity and cell abscission during cytokinesis. *Mol. Biol. Cell* **17**, 3881–3896
33. Reinecke, J. B., Katafiasz, D., Naslavsky, N., and Caplan, S. (2015) Novel functions for the endocytic regulatory proteins MICAL-L1 and EHD1 in mitosis. *Traffic* **16**, 48–67
34. Kouranti, I., Sachse, M., Arouche, N., Goud, B., and Echard, A. (2006) Rab35 regulates an endocytic recycling pathway essential for the terminal steps of cytokinesis. *Curr. Biol.* **16**, 1719–1725
35. Dambournet, D., Machicoane, M., Chesneau, L., Sachse, M., Rocancourt, M., El Marjou, A., Formstecher, E., Salomon, R., Goud, B., and Echard, A. (2011) Rab35 GTPase and OCRL phosphatase remodel lipids and F-actin for successful cytokinesis. *Nat. Cell Biol.* **13**, 981–988
36. Goss, J. W., and Toomre, D. K. (2008) Both daughter cells traffic and exocytose membrane at the cleavage furrow during mammalian cytokinesis. *J. Cell Biol.* **181**, 1047–1054
37. Gromley, A., Yeaman, C., Rosa, J., Redick, S., Chen, C. T., Mirabelle, S., Guha, M., Sillibourne, J., and Doxsey, S. J. (2005) Centriolin anchoring of exocyst and SNARE complexes at the midbody is required for secretory-vesicle-mediated abscission. *Cell* **123**, 75–87
38. Grigoriev, I., Splinter, D., Keijzer, N., Wulf, P. S., Demmers, J., Ohtsuka, T., Modesti, M., Maly, I. V., Grosveld, F., Hoogenraad, C. C., and Akhmanova, A. (2007) Rab6 regulates transport and targeting of exocytotic carriers. *Dev. Cell* **13**, 305–314
39. Neef, R., Klein, U. R., Kopajtich, R., and Barr, F. A. (2006) Cooperation between mitotic kinesins controls the late stages of cytokinesis. *Curr. Biol.* **16**, 301–307
40. Peränen, J., Auvinen, P., Virta, H., Wepf, R., and Simons, K. (1996) Rab8 promotes polarized membrane transport through reorganization of actin and microtubules in fibroblasts. *J. Cell Biol.* **135**, 153–167
41. Kao, A., Chiu, C. L., Vellucci, D., Yang, Y., Patel, V. R., Guan, S., Randall, A., Baldi, P., Rychnovsky, S. D., and Huang, L. (2011) Development of a novel cross-linking strategy for fast and accurate identification of cross-linked peptides of protein complexes. *Mol. Cell. Proteomics* **10**, M110.002212